6-22-2021

Effects of stiffness and cell shape on cellular mechanosensing

Sarah Lynn Furman
Rowan University

EFFECTS OF STIFFNESS AND CELL SHAPE ON CELLULAR MECHANOSENSING

by
Sarah Furman

A Thesis

Submitted to the
Department of Biomedical Engineering
College of Engineering
For the Degree of
Master of Science in Biomedical Engineering
at
Rowan University
May 5, 2021

Thesis Advisor: Sebastián L. Vega, Ph.D.

Committee Members:
Vincent Beachley, Ph.D.
Nichole Daringer, Ph.D.

Acknowledgements

I would like to thank Dr. Sebastian Vega for his guidance and support on this project. The knowledge and skills I have gained working with him and the whole Vega lab will be immensely valuable in my future, and I am very grateful for that. I would like to thank Kirstene Gultian for her continued guidance and assistance in the laboratory, as well as Mehdi Benmassaoud for his skills synthesizing peptides. Another special thanks to Gatha Adhikari who has helped me perform these experiments.

Finally, I would like to thank my mother and father for their never-ending support, and my sister Katie for her encouragement and guidance.

Abstract

Sarah Furman
EFFECT OF STIFFNESS AND CELL SHAPE ON CELLULAR MECHANOSENSING
2020-2021
Sebastián L. Vega, Ph.D.
Master of Science in Biomedical Engineering

Cellular mechanosensing is the process of converting mechanical signals into biological responses. Stem cells are self-renewing cells with the potential to transform into specialized cell types – this differentiation process is influenced by cellular mechanosensing. Cells sense material stiffness, and stiffer environments result in increased cellular mechanosensing and preferential differentiation into bone-producing osteoblasts. Cell shape also plays an important role due to its influence on cytoskeletal contractility, and photopatterning can be used to study the effects of cell shape on cellular mechanosensing. Although the effects of material stiffness and cell shape have been studied, little is known about the joint effects of these factors on stem cell mechanosensing. Taken together, the goal of this research is to develop a biomaterial system to study the combinatorial effects of shape and stiffness on mesenchymal stem cell (MSC) mechanosensing. Hydrogels of three stiffness (5 kPa, 10 kPa, 20 kPa) were photopatterned with shapes (circle, square, octagon) that cause a range of contractile forces in cells. These shapes were made into patterns on a glass photomask, allowing hydrogels placed under the photomask to be photopatterned. Photopatterns were found to over 90% accurate. Highly angular shapes, such as the octagon, and increased stiffness were both seen to influence an increased nuclear localization of mechanosensing protein YAP, with stiffness having a greater influence than shape.

Table of Contents

Table of Contents (Continued)

List of Figures

Chapter 1

Introduction

1.1 Stem Cells Overview

Stem cells are cells with the ability to self-renew and differentiate into different types of cells [1]. Unlike other cells, they do not carry out specific functions and instead wait for differentiation cues to become more specialized cell types [2]. There are three main class of stem cells: embryonic stem cells, adult stem cells, and induced pluripotent stem cells (iPSCs)[3]. Embryonic stem cells have the ability to differentiate into any somatic cell type, making them highly valuable to regenerative medicine research [4], [5]. However, they are only found during early embryonic development. This makes acquisition and use of embryonic stem cells controversial and expensive [4], [6].

Adult stem cells are more common and can be found throughout the body for the duration of one's life. These stem cells are multipotent, they belong to certain tissues and possess the ability to differentiate into a select few cell types of that tissue [7],[8]. There are three main types of adult stem cells: neural stem cells (NSCs), mesenchymal stem cells (MSCs), and hematopoietic stem cells (HSCs). Neural stem cells are found in regions of the brain and spinal cord and give rise to neurons and glia cells[9]. Preliminary work has been done on these adult stems as a therapeutic for neurodegenerative disease [10]. MSCs are found many areas of the body including in bone marrow and are responsible for formation of connective tissue such as bone, fat, and cartilage [11], [12]. Studies of MSCs have shown great hope in bone and cartilage regrowth if the MSC differentiation can be controlled [13], [14] The final type of adult stem cells, HSCs, are also found in bone marrow and give rise to a variety of immune and blood cells [15]. The

multipotency of adult stem cells makes them ideal for personalized and regenerative medicine if their differentiation can be understood and controlled.

Induced pluripotent stem cells are not found in the body, but instead engineered in vitro. These types of stem cells are previously differentiated cells that have been reprogramed to behave as embryonic stem cells. This is done though the introduction of certain genes to change the properties of these cells [16]. The discovery of iPSCs has led to new techniques for studying disease models, personalized medicine, and cellular based therapies [17]. Reprogramed patient derived somatic iPSCs have been proven to be non-immunogenic [18] and current studies are working to lower cost and efficacy of patient derived iPSC production for medical use [19].

Outside of the body, stem cell behavior can be manipulated via local cues that include cell-cell contact and cellular interactions with engineered materials. For example, control of key chemical and physical factors can lead towards guided stem cell differentiation. Biochemical cues presented as ligands tethered to biomaterials and biophysical cues including substrate stiffness have a tremendous impact on cellular mechanosensing and downstream differentiation [20]. Understanding the effects of different biochemical and biophysical cues creates a diverse understanding of stem cell differentiation and control.

1.2 Soft Biomaterials for Stem Cell Culture

In order to better understand stem cell differentiation, biomaterials can be used [21]. Biomaterials are any material that can be used with biological matter including tissues and cells. This is a broad spectrum of materials which includes metals used in surgical implants, contact lenses that improve sight, and hydrogels used for laboratory cell culture [22]. Hydrogels are water based three dimensional gels developed specifically for

integration with cells. They can be created from a variety of polymeric materials including poly (ethylene glycol), polyacrylamide and hyaluronic acid. Hydrogels were the first material made specially for cell and tissue integration and as such they have many tunable properties including porosity, stiffness, and gelation time [23]. These factors and their similarity to native tissues make hydrogels a suitable biomaterial for studying artificial cellular microenvironments [24]. Hydrogel stiffness can be varied to mimic different tissue types and inclusion of cellular adhesion complexes allows easy cell seeding onto hydrogels. These easily tunable factors offer a platform to study specific cells in environments mimicking those the cells would encounter in vivo [25]. This can provide valuable information about cell behavior, and in the case of stem cells, differentiation. Addition of specific growth factors [26], tethering of functionalized molecules to hydrogels [27], and differing gel stiffness [28] have all been shown to influence MSCs to preferentially differentiate into osteoblasts as opposed to adipocytes. Understanding and control of stem cells through biomaterials offers potential for developments in regenerative medicine as well as individualized therapeutics [29].

1.3 Cellular Mechanosensing

1.3.1 How Cellular Mechanosensing Works

Cells possess the ability to convert mechanical signals into biological signals via a process known as cellular mechanosensing. This process controls cytoskeletal contractility and cell adhesion to an underlying substrate or nearby cells [30]. Cellular mechanosensing occurs through a number of force sensing proteins found in the extracellular matrix (ECM) [31] as well as through focal adhesion [32], [33]. Focal adhesions are proteins which adhere cells to their underlying substrate. Stiffer

environments lead to large cells with more focal adhesions and more organized cytoskeletal structures than cells on softer environments. This physical response to mechanosensing is responsible for large scale tissue changes such as muscle growth due to stress and strain on cells after exercise as well as bone formation based on an individual's weight distribution [34]. In stem cells, mechanosensing impacts cell differentiation [28], [35], [36]. Increased nuclear localization of mechanosensitive proteins, such as Yes-associated protein (YAP), have been linked to high cytoskeletal contractility after growth on a stiff substrate. YAP is regularly found throughout the cytoplasm of a cell but can be translocated to the nucleus where it plays a role in a signal cascade responsible for differentiation into contractile cell types (e.g., osteoblasts). The differences in YAP location on different stiffnesses can be seen in Figure 1. Due to YAP translocation and downstream effect on signaling, an increase in nuclear YAP concentration is known to increase rates of osteogenesis in MSCs, while lower nuclear YAP concentrations more often lead to adipogenesis [37].

Figure 1

YAP Location in Cells

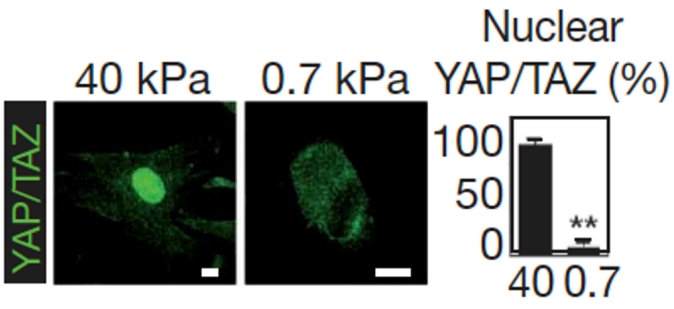

Note. Stiffer 40 kPa substrate on left shows greater nuclear YAP (green) than its 0.7 kPa counterpart. [Figure amended from Dupont et al 2011].

1.3.2 Factors Influencing Cellular Mechanosensing

An important aspect of cellular mechanosensing is substrate stiffness. The stiffness of the biomaterial a cell is placed on can affect the translocation of mechanosensitive protein YAP within a cell [38] and further downstream stem cell differentiation [30], [39]. Cells plated on soft materials similar to brain tissue are more likely to undergo neurogenesis while those on stiff materials mimicking bone are more likely to undergo osteogenesis [28]. In MSCs specifically, soft substrates lead to lower levels of nuclear YAP (Figure 2A) and higher likelihood of adipogenesis while stiff substrates lead to high nuclear YAP concentrations and osteogenesis [36].

Additionally, cell shape can influence mechanosensing and YAP translocation from the cytosol to nucleus of a cell. Cell shape influences the placement of focal adhesions and contractility [30], [40]. MSCs plated on angular shapes tend to create focal adhesions at the vertices of the shape. The cytoskeleton reflects these focal adhesions with increased contractility between adhesions and overall higher nuclear expression of YAP [30] [41]. In rounder shapes, less numerous and less distinct focal adhesions are created and overall cytoskeletal contractility is low, relating to low levels of nuclear YAP [30]. (Figure 2B) As was seen with stiffness, low levels of nuclear YAP correlate to MSC adipogenesis and high levels to osteogenesis [41].

Figure 2

Overview of Expected Impact on Mechanosensing

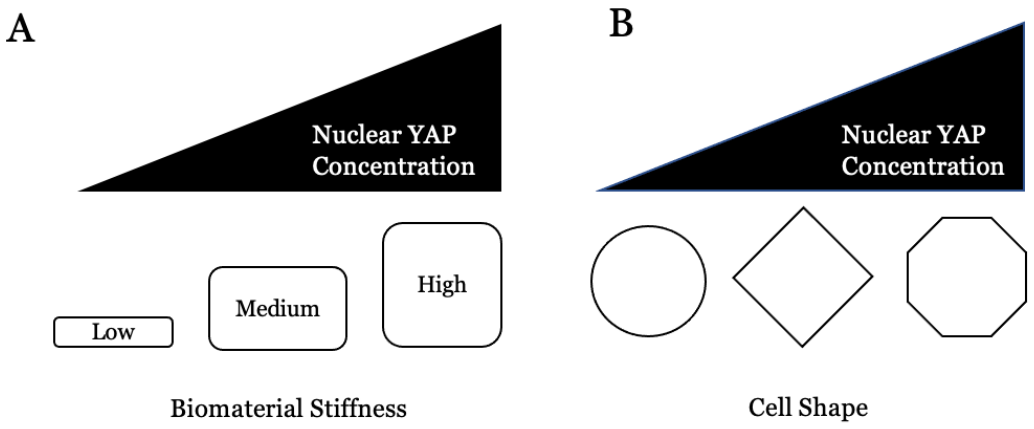

Note. (A) Increasing biomaterial stiffness is expected to increase mechanosensing and (B) increasing shape angularity and number of vertices is expected to increase nuclear YAP concentration.

1.3.3 Limitations in Cellular Mechanosensing Studies

While the effects of stiffness and shape on mechanosensing have been characterized independently, no studies have looked into them together. Matrix stiffness studies have shown preferential differentiation of MSCs on polyacrylamide hydrogels to be neurogenic on 0.1-1 kPa, myogenic on 8-17 kPa, and osteogenic on 25-40 kPa stiffnesses based on expression of preliminary differentiation markers β3 tubulin, MyoD1, and CBFx1 respectively [28]. Additionally, studies of shape done on patterned, gold-plated glass used a rounded flower and 5 point star to prove that more angular shapes increase cytoskeletal contractility and osteogenic differentiation [41]. Larger shapes are also seen to have higher nuclear YAP concentrations, as are MSCs on stiffer substrates [42]. Compilation of these studies indicates that both increased stiffness and use of angular

shapes should result in high nuclear levels of mechanosensing protein YAP and downstream osteogenic differentiation.

Here I am to create a biomaterial system to characterize the effect of substrate stiffness and cell shape on MSC mechanosensing through nuclear YAP translocation. A hydrogel of tunable stiffness will allow for distinct characterization of nuclear YAP based on stiffness. The same hydrogel can be patterned with shapes of varying angularity to determine shape effect on nuclear YAP concentrations. Combinatorial results of these two factors on nuclear YAP can provide better indications of their effect on mechanosensing and further downstream cell differentiation.

Chapter 2

Designing Hydrogels with Tunable Stiffness and Orthogonal Micropatterning

2.1 Introduction

2.1.1 A Hydrogel System for Micropatterning

To better understand mechanosensing, first a substrate and patterning system was needed. Hydrogels were chosen due to their biocompatibility and ability to tune hydrogel stiffness [25]. Hydrogels made would then need to be patterned using a photomask for studies of shape. Different hydrogel bases such as polyacrylamide and hyaluronic acid were considered as both have shown success in patterning [41], [43]. Initial work with polyacrylamide gels showed incorrect transfer of pattern from photomask to hydrogel. This led to the decision to use norbornene modified hyaluronic acid hydrogels which have been shown to allow orthogonal patterning after synthesis with ease [43].

2.1.2 Norbornene Modified Hyaluronic Acid

Norbornene modified hyaluronic acid (NorHA) is a macromer made by combining norbornene and hyaluronic acid. This macromer can act as a backbone for the creation of hydrogels. The norbornenes attach to hyaluronic acid chains and have a high affinity for thiol molecules. Di-thiol molecules are able to attach to two separate norbornenes to crosslink or join different strands of NorHA together. This thiol-norbornene reaction occurs in the presence of a photo initiator and ultraviolet (UV) light. Due to the simplicity of the thiol-norbornene binding, hydrogel stiffness can be easily controlled [43], [44]. NorHA combined with high concentrations of di-thiol molecules tightly bind together and create a stiffer gel, while lower di-thiol concentrations loosely link macromers and create softer gels.

The thiol-norbornene reaction can also be used to micropattern hydrogels after their formation. This is done with functionalized single thiol molecules, instead of di-thiol molecules. These molecules have a thiol group attached to a peptide which is then bound to free NorHA in already formed NorHA hydrogels. The reaction occurs the same way, by introducing a thiol molecule to the NorHA in the presence of a photo initiator and UV light.

2.1.3 Micropatterning

Micropatterning allows for the creation of distinct cellular adhesive regions on a biomaterial in order to study cell microenvironments [45] Micropatterning can be done using a photomask [46]. The photomask acts as a template, allowing light to shine through in predetermined areas. In the case of NorHA hydrogels, the functionalized thiol molecules adhere to norbornene in the presence of UV light. By shining UV light through the photomask with a hydrogel underneath, the hydrogel becomes patterned with the design of the photomask. If the thiol molecules used are functionalized with fluorescence, then the patterns can be visualized with fluorescent imaging. This patterning technique can also be used to spatially functionalize hydrogels with cell attachment motifs (i.e., RGD) to create adhesive regions for cells to attach to. Since no further crosslinking is occurring, patterning does not change the local stiffness of a NorHA hydrogel [43].

2.2 Materials and Methods

2.2.1 NorHA Synthesis

To create NorHA, Hyaluronic Acid tetrabutylammonium salt (HA-TBA) was combined with Nor-amide and dissolved in dimethyl sulfoxide (DMSO) at a concentration of 5 mL per 0.1g via cannulation. Benzotriazole-1-yl-oxy-tris-

(dimethylamino)-phosphonium (BOP) was added to a new beaker and combined with dissolved DMSO solution via cannulation. Once dissolved, the reaction continued at room temperature for 2 hours. 10 mL of DI water was added, and the solution was transferred to dialysis tubing. Dialysis occurred for 5 days at room temperature with water changes twice a day. The resulting solution was filtered and dialyzed for 3 more days. It was then frozen overnight at -80 C and lyophilized for 5 days. H NMR was used to analyze the final NorHA macromer.

2.2.2 NorHA Hydrogel Formation

NorHA hydrogels were created in silicone molds. The NorHA macromer, Di-thiol cross linker (DTT), and a photoinitiator were combined with PBS to create a gel solution (Figure 3). This solution was then injected into molds. The molds were created by cutting 10 mm diameter circles out of silicone and placing them on top a 12 mm diameter coverslip. The solution was injected into the mold then covered with another 12 mm coverslip and exposed to UV light for 10 minutes at 10 milliwatts/cm^2. The hydrogels attached to a single coverslip were them removed from the mold and soaked in PBS.

Figure 3

NorHA Formation

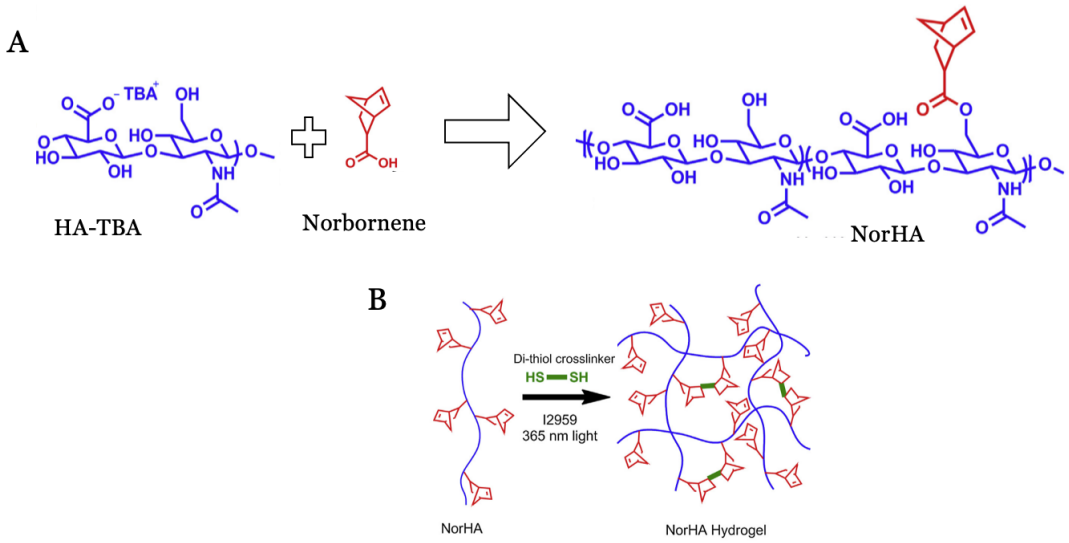

Note. (A) Synthesis of NorHA from HA-TBA and norbornene via a click chemistry reaction. (B) Crosslinking of NorHA macromer with Dithiol crosslinker to create a hydrogel. [Figure amended from Gramlich et. al 2013].

2.2.3 Photomask Design

To micropattern the NorHA hydrogels, a photomask was designed. The photomask was designed with three shapes, a circle, square, and octagon in mind. The lack of vertices on a circle would be expected to cause low contractile forces and result in adipogenesis. In contrast, an octagon is highly angular and would significantly increase the contractile force felt by a cell leading to osteogenesis. A square was chosen as an intermediate shape to these two extremes, creating cells with moderate contractile forces. Each of these shapes was designed with an area of 5,000 μm^2 based on previous successful patterning and the known size of MSCs [41] (Figure 4A). Consistency in

shape area allows the study of cell shape independent of size. The shapes were designed in repeating iterations on AutoCAD with each shape in one third of an 18-millimeter diameter circle (Figure 4B). This allows for rapid patterning of all three shapes onto one substrate. The completed AutoCAD design was sent to CompuGraphics who created a glass photomask that can be used for micropatterning.

Figure 4

Photomask Design

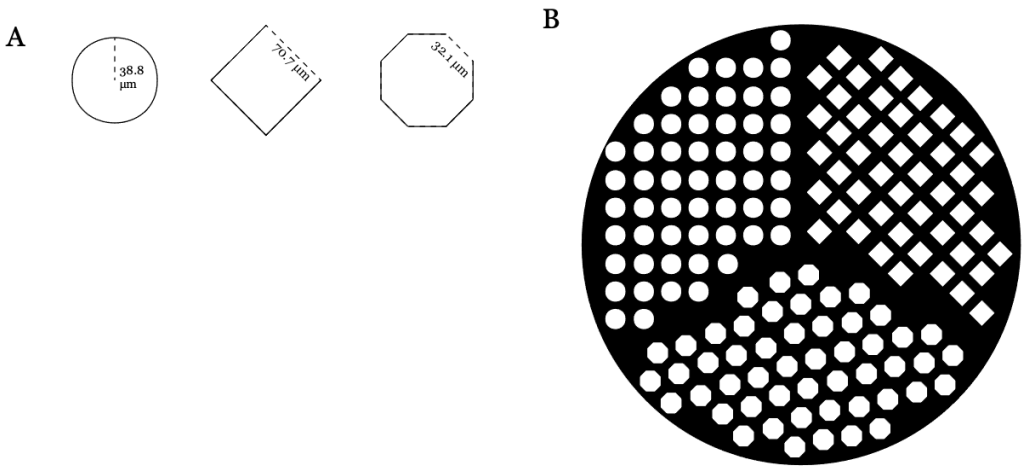

Note. (A) Length of three shapes chosen for the photomask. (B) Overview of the photomask showing all three shapes repeating with in one circle.

2.2.4 Photopatterning NorHA Hydrogels

The previously created NorHA gels were soaked in a patterning solution consisting of cell adhesion peptide RGD, photoinitiator, and PBS. For pattern fidelity testing, thiolated green florescent protein was added to this solution. The hydrogels were removed from the solution and placed on the bottom side of the glass photomask via PBS adhesion. The

photomask was flipped right side up and placed on a stand. UV light at the same intensity as before was shone on the mask through the gel to create micropatterns (Figure 5). Gels were imaged to ensure transfer of the pattern (Figure 6).

Figure 5

Schematic of Patterned Hydrogel Creation

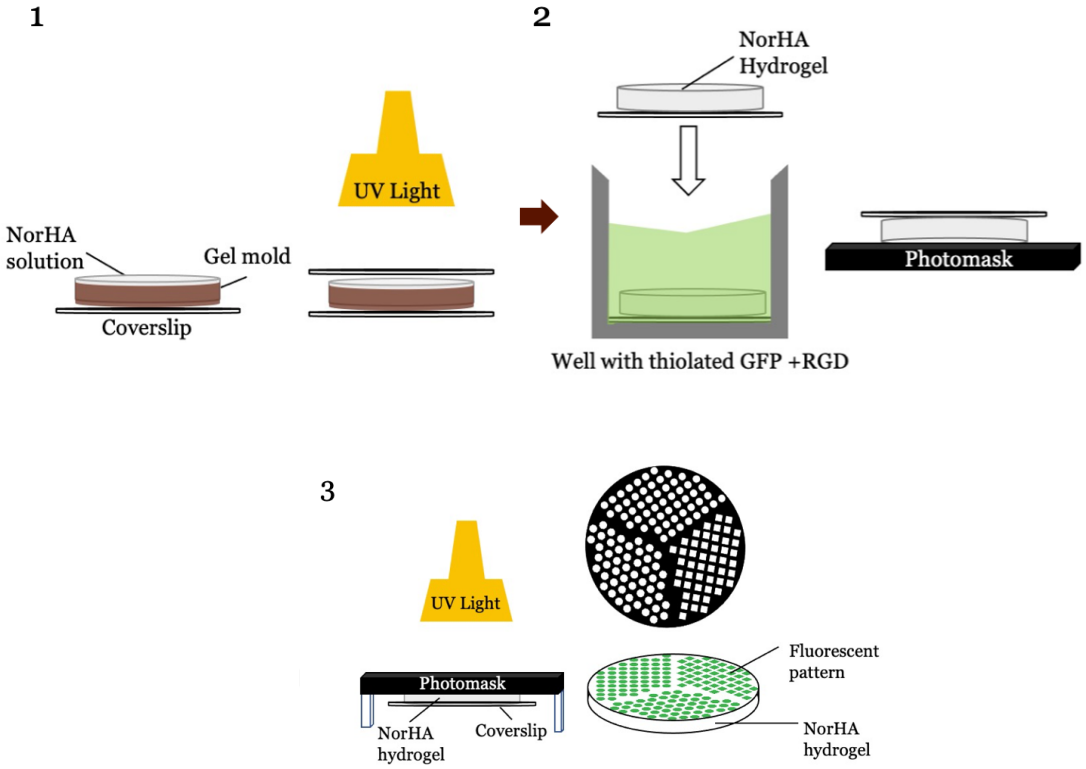

Note. (1) The NorHA solution is loaded into a mold sandwiched between two coverslips and exposed to UV light. (2) After creation, the hydrogel is soaked in a solution of RGD and fluorescent peptide then placed on the photomask. (3) The photomask and hydrogel are placed under UV light for 5 min. Once removed from the UV light the result is a fluorescently patterned hydrogel matching the photomask design.

Figure 6

Visualization of Photopatterned Shapes

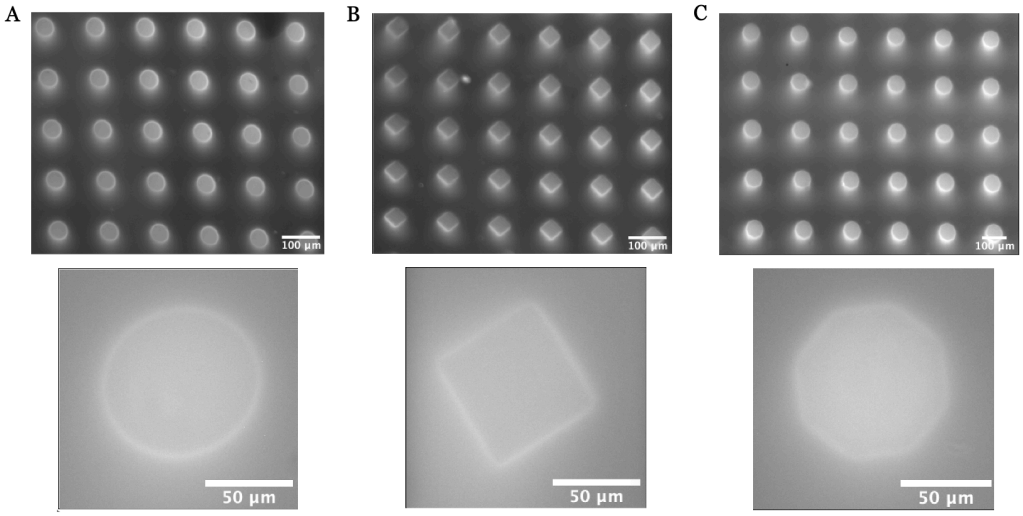

*Note***.** Images of multiple and single patterns for (A) circles, (B) squares, (C) octagons.

2.3 Results and Discussion

2.3.1 NorHA Hydrogels of Varying Stiffness Were Created

NorHA hydrogels of three different stiffnesses were desired for testing the effect of stiffness on mechanosensing. NorHA stiffness was varied using different concentrations of the crosslinker dithiothreitol (DTT) during creation of the NorHA hydrogels. Variation in DTT allows more precise changes in stiffness than varying the weight percent of NorHA in the hydrogel [43]. Tested DTT concentrations resulted in a range of stiffness from 5-25 kPa (Figure 7A). Test concentrations below 1 mM DTT resulted in poorly formed hydrogels that did not hold their shape. The plateau seen between 3 and 5 mM DTT is likely the result of a reaction threshold where all norbornenes are crosslinked to a thiol. Increasing DTT concentration past 3 mM would not be expected to have any significant increase on stiffness.

Stiffnesses were selected at a low, medium, and high stiffness corresponding to 5, kPa, 10 kPa, and 20 kPa (Figure 7B). Adipose tissue has a young modulus of 1.9 kPa [47] and adipogenesis is known to occur on substrates between 2.5-5 kPa [48]. For that reason, the lowest stiffness was chosen as 5 kPa with the expectation of low mechanosensing. While the young's modulus of bone is extremely high, ranging from 20-22 GPa [49], osteogenesis has been successfully induced in hydrogels of 20-40 kPa [28] leading to the choice of a high 20 kPa stiffness. 10 kPa was then chosen as an intermediate stiffness to the low 5 kPa and high 20 kPa. Based off tested DTT concentrations, these low, medium, and high stiffnesses were found to correspond to 1 mM, 1.75mM, and 2.5 mM DTT concentrations, respectively.

Figure 7

NorHA Hydrogel Stiffness

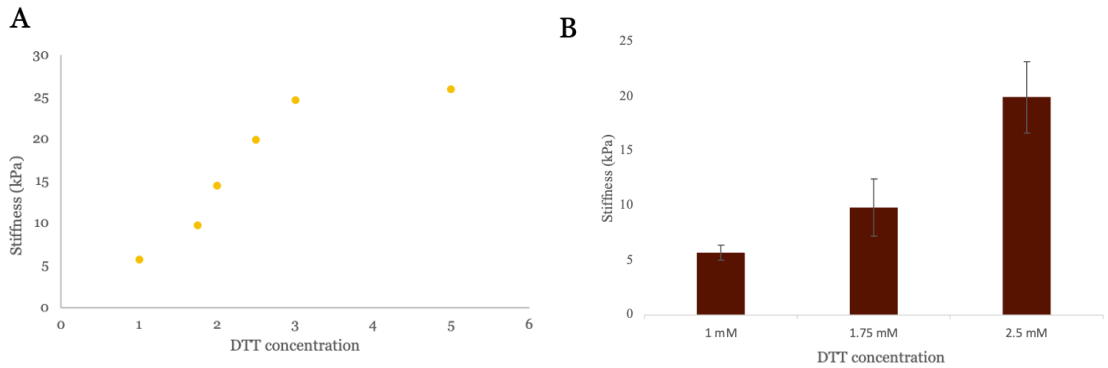

Note. (A) Stiffness of all tested DTT concentrations. N=6 for each concentration. (B) Chosen concentrations of 1 mM, 1.75 mM, and 2.5 mM DTT to for 5 kPa, 10 kPa, and 20 kPa stiffness, respectively. Concentrations were chosen based of off graph A.

2.3.2 Micropatterns Were Made on NorHA Hydrogels with High Fidelity

The fidelity of each different pattern was examined using FIJI. Fluorescent patterning was done with 0.001 mM of thiolated GFP as lower concentrations became hard to visualize and higher concentrations resulted in over saturation when imaging. Images of 30 patterns were measured for shape length and area and compared to the known pattern size of the photomask (Figure 8). Circular fluorescent patterns were found to have an average size of 4433.53 μm^2 making them 6% smaller than the photomask pattern. Square and octagon fluorescent patterns were both less than 4% smaller than the photomask pattern at 4817 and 4805 μm^2, respectively. The pattern accuracy ratio of measured patterned length or area to actual length or area was plotted with a box plot for 30 samples of each shape (Figure 9). Median pattern accuracy ranged from 0.9 to 0.98 for length and 0.94 to 0.97 for pattern area where 1 indicates a measured fluorescent pattern the same size as the photomask pattern. On average, fluorescent patterns were 95.6% the area of the photomask pattern. It would be expected that other patterns using the same method would be equally as accurate. The combined stiffness and pattern fidelity results indicate a working biomaterial for creating NorHA gels of varying stiffnesses with micropatterns.

Figure 8

Visual Comparison of Patterned Hydrogel and Photomask

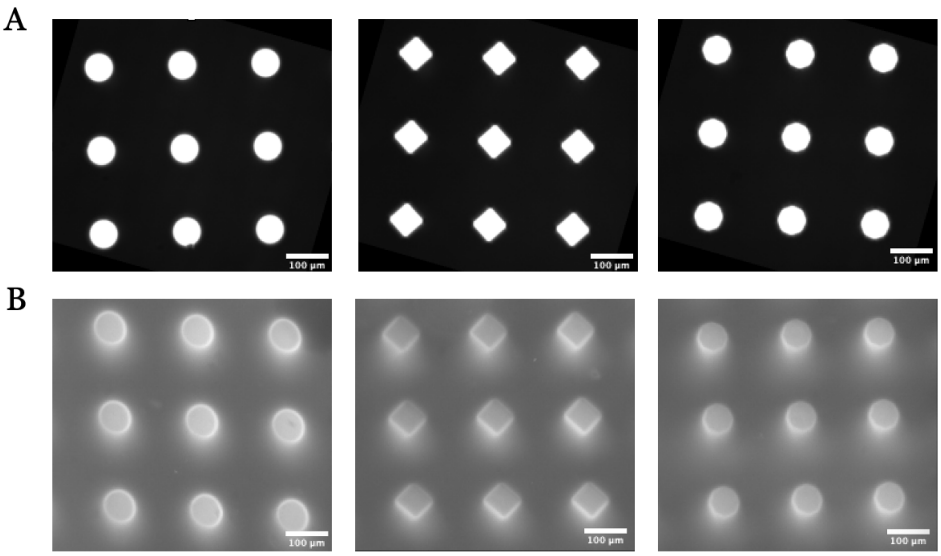

Note. (A) Images of photomask itself compared to (B) corresponding patterned hydrogels.

Figure 9

Pattern Fidelity

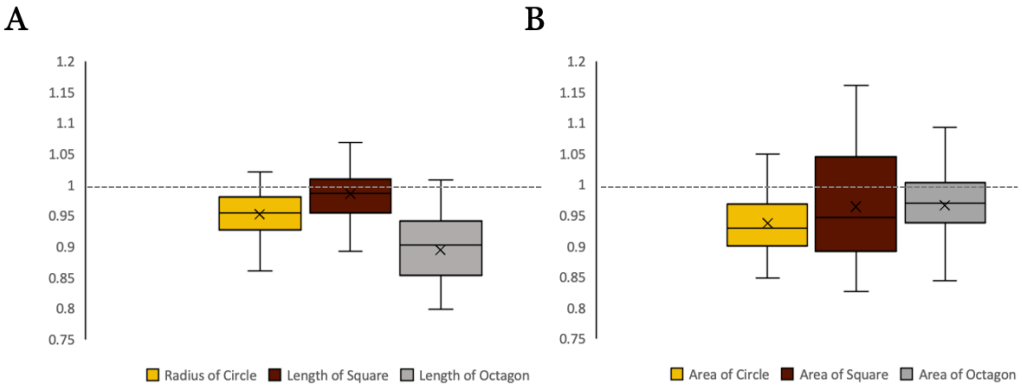

Note. Accuracy of patterning seen in box plot comparing measured (A) pattern length and (B) pattern area to known photomask parameters for confocally imaged patterned hydrogels. Mean pattern accuracy is indicated with an x where 1, shown with a dotted line, represents the measured pattern exactly equal to the photomask pattern. Patterns above the dotted line were larger than the photomask and below were smaller than the photomask. Done on 5 kPa NorHA hydrogels for an n=30.

Chapter 3

MSC Seeding onto Micropatterned Hydrogels

3.1 Introduction

3.1.1 MSC Overview

Mesenchymal stem cells can differentiate into osteoblasts to create bone, adipocytes to create fat tissue, and chondrocytes to create cartilage [50]. They are relatively easy to grow and culture in a laboratory [51], and show promise in controlled differentiation and use in regenerative medicine. Understanding of MSC differentiation has potential to lead to the ability to regenerate and repair cartilage and bone tissue for injury or disease treatment [52]. MSCs have been proven to have to no adverse effects when used in clinical trials [53], but control and understanding of their differentiation is not well understood. Many properties including transcription factors, cell-cell signaling, and mechanosensing influence MSC differentiation [54]. Better investigation of how these factors influence differentiation is needed to advance regenerative uses [55].

3.1.2 Role of Mechanosensing in Differentiation

Increased levels of mechanosensing have been correlated to osteogenic differentiation with MSCs [30]. Control of MSCs through shape has been done on rounded and angular shapes. Angular shapes show increased cytoskeletal contractility indicating high levels of mechanosensing as well as increased levels of osteogenic differentiation markers [41]. This has led to the choice of an octagon, square, and circle for this study. These shapes are expected to have a range of mechanosensing with circles being the lowest and octagons being the highest. When MSCs are cultured on stiff 22 kPa substrates, they also have higher expression of mechanosensing than those cultured on

soft 3.6 kPa substrates [36]. A range of stiffness (5 kPa, 10 kPa, and 20 kPa) have been chosen to study in conjunction with the three shapes. These varying shapes and stiffnesses are expected to varying mechanosensing within the cell leading to changes in levels of osteogenic and adipogenic differentiation.

3.2 Materials and Methods

3.2.1 MSC Culture

Lonza bone marrow derived MSCs with passage numbers ranging from P3-P6 were used for seeding. Cells were cultured in Gibco alpha minimum essential media constituted with penicillin and streptomycin and 10% fetal bovine serum. Cells were passaged at 80% confluency. Cells were rinsed with sterile Gibco PBS and treated with trypsin for 5 minutes in a cellular incubator. Media was proportionally added to neutralize the trypsin. The cell solution was centrifuged at 500 x g for 5 minutes. The supernatant was aspirated off and the cell pellet resuspended in media. Cells were counted with a hemocytometer and seeded onto hydrogels with varying density or replated for future use.

3.2.2 MSC Seeding Conditions

Micropatterned NorHA Hydrogels in a 24 well plate were washed with PBS then seeded at different densities to optimize pattern adhesion. Both a low and high centrifuge and seeding density was tested. Cells were seeded at either 3,000 cells/cm^2 or 5,000 cells/ cm^2 and then centrifuged at 300x g or 500x g.

3.2.3 Cell Staining

Cells were fixed with 10% formalin 24 hours after seeding. Fixed cells were washed with PBS, permeabilized, and then blocked for 30 minutes using 3% bovine serum

albumin. Following this, a 1:200 concentration of Santa Cruz YAP was made in PBS and 50 microliters droplets were placed on a parafilm lined petri dish. Gels were placed, cell side down, on the drops and incubated at room temperature for 1 hour. Gels were then washed 5x and placed on 50 microliters droplets of 1:200 Alexa Fluor anti-mouse IgG antibody where they were incubated in the dark for 2 hours. Once finished, gels were moved to a new 24 well plate and washed 5 times with PBS. They were then soaked in a 1:200 Alexa Fluor 488 phalloidin-blocking buffer solution, washed and soaked in a 1:5000 Hoechst – PBS solution. Stained hydrogels were washed with PBS and stored in 4 degrees Celsius until imaging.

3.2.4 Imaging and Analysis

Images of micropatterned hydrogels were taken using Nikon confocal microscopy. 20x images of cells representing circle, squares, and octagons were taken. 8-bit images were analyzed in FIJI for YAP concentration. The fluorescent intensity of three 3x3 squares was measured in the nucleus and cytoplasmic area of each cell. The average of these measurements was separately taken for the nucleus and cytoplasm of each cell and divided to find the nuclear to cytoplasmic YAP ratio.

3.2.5 Statistical Analysis

Statistical analysis was done with an ANOVA test followed by t-test assuming equal variances where relevant.

3.3 Results and Discussion

3.3.1 Cells Seeded at High Density and High Centrifuge Speed

Two cell seeding densities and two centrifuge speeds were tested to determine optimal cell seeding conditions. The cells seeded at 5,000 cells/ cm^2 and centrifuged at

500x g had the most single cells adhered in patterns and these conditions were used for future testing. Other combinations of conditions resulted in few cells adhering to patterns. Further testing of higher cell seeding conditions (7500 cell/cm^2 and 10000 cells/cm^2) lead to multiple cells adhering to a single pattern instead of the desired single cell per single pattern. With the chosen density of 5,000 cells per cm^2, some cells were seen adhered randomly outside of patterns. To combat this a wash using bovine serum albumin (BSA) could be added directly after patterning the hydrogels. This would create a less favorable environment for the cells on any area of the gel that is not patterned and possibly increase the number of single cells correctly adhered to a pattern.

Three time points were also testing by fixing cells at 24, 48, and 72 hours. At both 48 and 72 hours many cells were adhered on and around a single pattern making characterization of single cells in patterns impossible (Figure 10). The fluorescent patterns were also seen to be bleeding into surround gel. This inaccuracy in pattern size is likely due to the long periods of times the gel was in cell media for these time points. Bleeding of patterns could also indicate bleeding of adhesion motif RGD which would be responsible for the high number of cells outside of patterns. At 24 hours single cells were properly adhered to the constraints of the pattern and this time point was used for all other testing.

Figure 10

72-Hour Cell Seeding Study

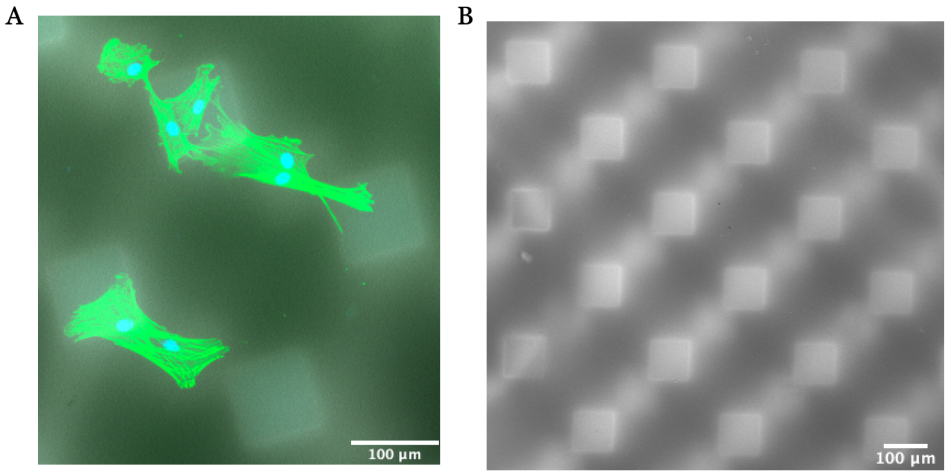

*Note***.** (A) Cells seeded on patterns and fixed 72 hours after seeding showed multiple cells per pattern and (B) fluorescence bleeding out of patterned areas.

3.3.2 Characterization of Mechanosensing

YAP is a mechanosensing protein responsible for transmitting mechanical signals obtained from the extracellular matrix to a cell's nucleus [38]. This signal relay activates the hippo-pathway which is responsible for regulating stem cell fate and proliferation [56], [57]. Higher nuclear YAP concentration is linked to osteogenesis while lower nuclear YAP and higher cytosolic YAP concentrations are indicative of adipogenesis in MSCs[6]. Here YAP has been used to quantify mechanosensing. Cells plated on different shapes show different YAP localization (Figure 11). Cells on circular shapes exhibited spread out YAP concentrations with little difference in nuclear and cytoplasmic YAP. Squares also had cytoplasmic YAP, but their nuclear YAP concentrations were distinctly higher than cytoplasmic concentrations. On the contrary cells in octagons showed almost

exclusively nuclear YAP with very little cytoplasmic YAP. To Quantify mechanosensing, YAP ratio was used (Figure 12). This ratio, based of fluorescent intensity, shows the level of nuclear YAP compared to that of the cytoplasm for a normalized ratio indicative of nuclear YAP concentrations and mechanosensing.

Figure 11

Images of the Cytoskeleton, Nucleus, YAP, and Combined Channels for the Circle, Square and Octagon

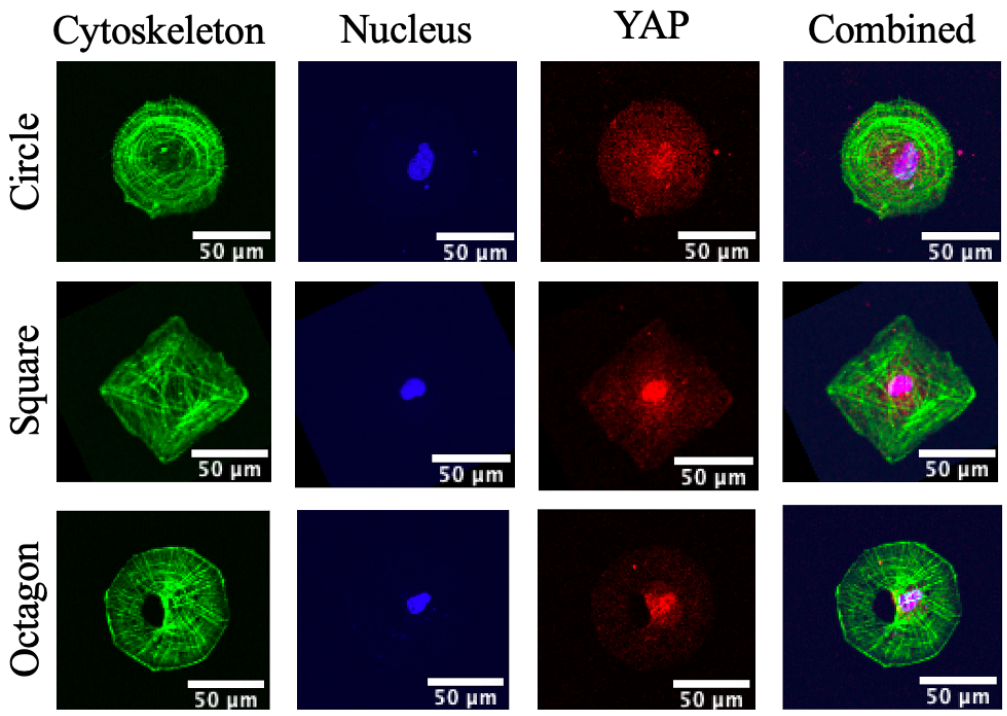

Note. Stained for Phalloidin (green) showing the cytoskeleton, Hoechst (blue) showing the nucleus, and YAP (red). Images shown for the circle and square are on 10 kPa hydrogels, and the images of the octagon are on 20 kPa hydrogels. All cells were stained after 24 hours.

Figure 12

Calculation of YAP Ratio Based off Fluorescence of Nuclear and Cytoplasmic YAP

$$\frac{Average\ YAP\ flourescence\ in\ nucleus}{Average\ YAP\ flourescene\ in\ cytoplasm}$$

3.3.2.1 Mechanosensing Based on Shape. YAP ratio increased as angularity increased, with circles having the lowest ratio and octagons having the highest (Figure 13). On hydrogels of a medium stiffness, 10 kPa, squares had a YAP ratio 1.2x higher than circles and octagons had a YAP ratio 1.3x higher than circles. This confirms previous findings that increasing contractility in shapes increases mechanosensing. While there was significant difference between YAP ratios of circles and squares as well as circles and octagons, there was not large differences between that of squares and octagons. This may indicate that there is a contractility threshold based on shape. The contractile forces experienced by a cell with four vertices are not seen to be proportionally or significantly less than those of the forces experienced a more angular cell with 8 vertices.

Figure 13

YAP Ratio Compared to Tested Shapes

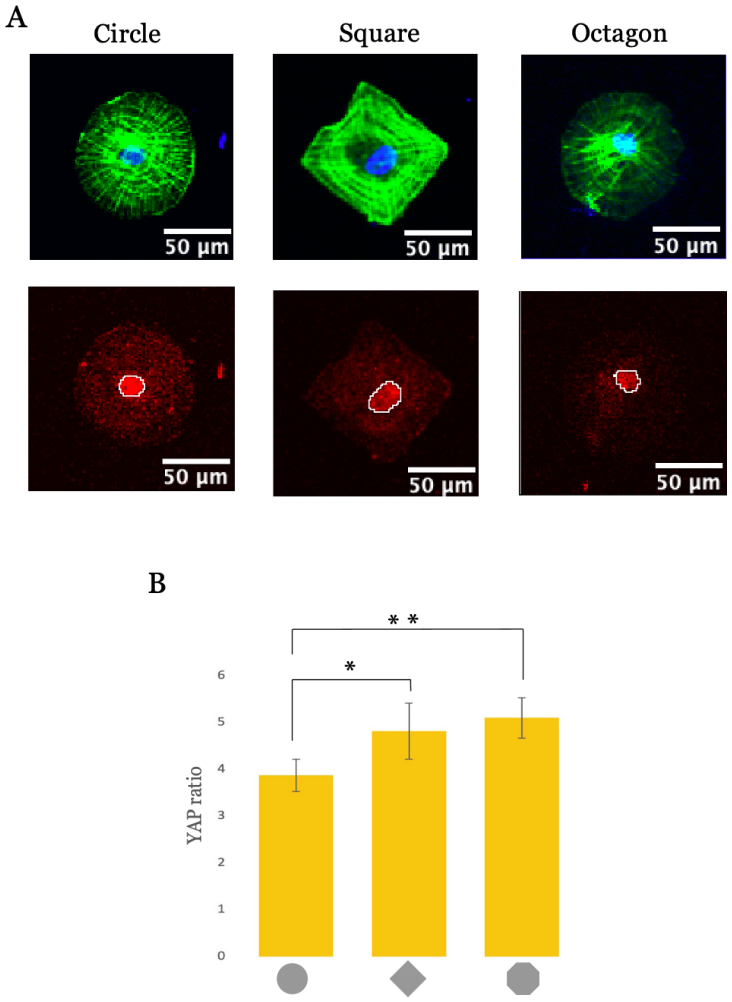

Note. (A) Increased YAP ratio was seen as shape angularity increased. Stained for phalloidin (green), Hoechst (blue) and YAP (red). For contrast, nucleus of YAP channel is outlined in white. (B)Plot of average YAP ratio in relation to shape. Hydrogels of 10 kPa stiffness were used. Significant differences denoted by * for the increase in YAP ratio from circle to square and ** for circle to octagon.

3.3.2.2 Mechanosensing based on Stiffness. All shapes experienced higher YAP ratios on stiffer NorHA hydrogels. Circles on 20 kPa hydrogels had YAP ratios 1.6x higher than those on 5 kPa hydrogels (Figure 14). Similarly, Octagons on 20 kPa hydrogels had YAP ratios 2.2x higher than their 5 kPa counterparts (Figure 15). At 20 kPa stiffness YAP localization can be seen as highly nuclear, with little cytoplasmic YAP visible in all shapes.

Figure 14

YAP Ratio Compared to Low, Medium, and High Stiffnesses for Circular Patterned Cells

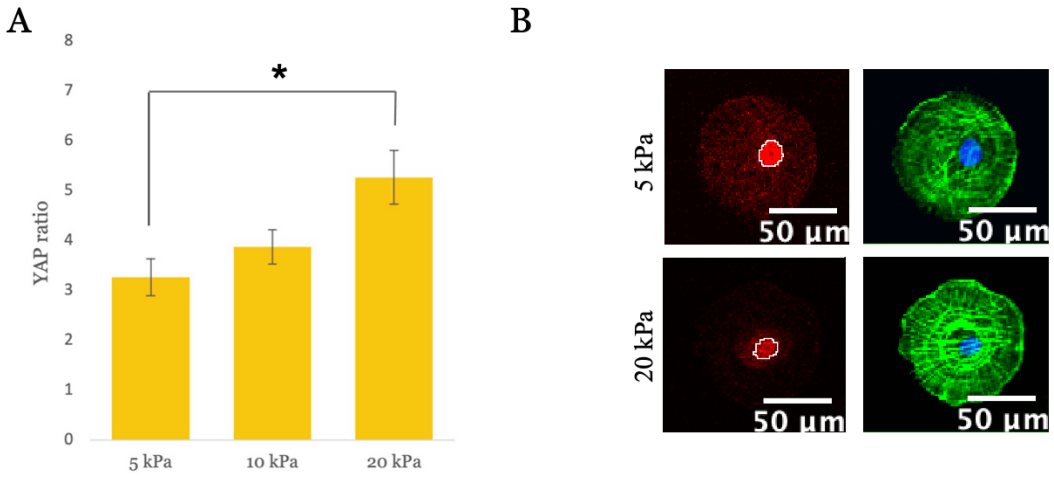

Note. (A) Significant increases can be seen in YAP ratio when plated on 5 kPa to 20 kPa hydrogels. This can be further seen in (B) YAP fluorescence being highly nuclear on 20 kPa. Cells pictured here are stained for phalloidin (green), Hoechst (blue) and YAP (red). Nucleus is outlined on YAP channel in white.

Figure 15

YAP Ratio Compared to Low, Medium, and High Stiffnesses for Octagonal Patterned Cells

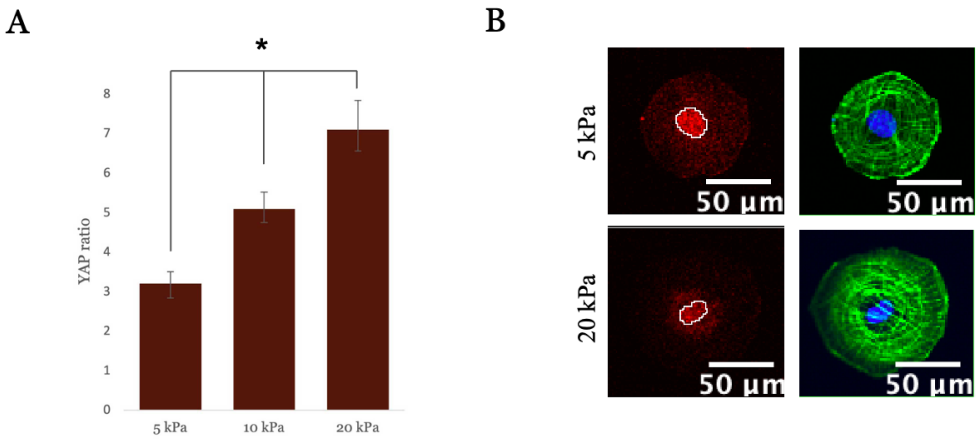

Note. (A) Significant increases can be seen in YAP ratio when plated on 5 kPa to 20 kPa hydrogels. This can be further seen in (B) YAP fluorescence being highly nuclear on 20 kPa. Cells pictured here are stained for phalloidin (green), Hoechst (blue) and YAP (red). Nucleus is outlined on YAP channel in white.

3.3.2.3 Combinatorial Effects of Shape and Stiffness on Mechanosensing.

Shape was seen to amplify the effect stiffness on YAP ratio. The YAP ratio of octagons increased with a greater slope than that of the circles when measured across the three stiffnesses (Figure 16A). Additionally, circles and octagons were seen to have significant YAP ratio increases from 5-20 kPa hydrogels while squares were not (Figure 16B). Without patterning, MSCs on soft hydrogels are generally small and circular while those on stiff hydrogels are elongated with clear focal adhesions [41]. Since the square is in between these two cell shapes, it is likely that it has an increased YAP ratio compared to small circular cells on soft gels but a decreased YAP ratio compared to spread cells on

stiff gels. This creates a medial YAP concentration for squares on both soft and stiff gels. While it would be expected that octagons would have higher YAP concentrations than squares on soft 5 kPa hydrogels, this was not observed. This phenomenon is likely due to the preferential shape of cells on soft gels. Cells seen in octagonal patterns on soft hydrogels were far more rounded than those seen on stiffer hydrogels (Figure 17). While they were still octagonal in shape, they had rounded edges which was not expected and could account for this difference.

Figure 16

Combinatorial Effects of Shape and Stiffness on YAP

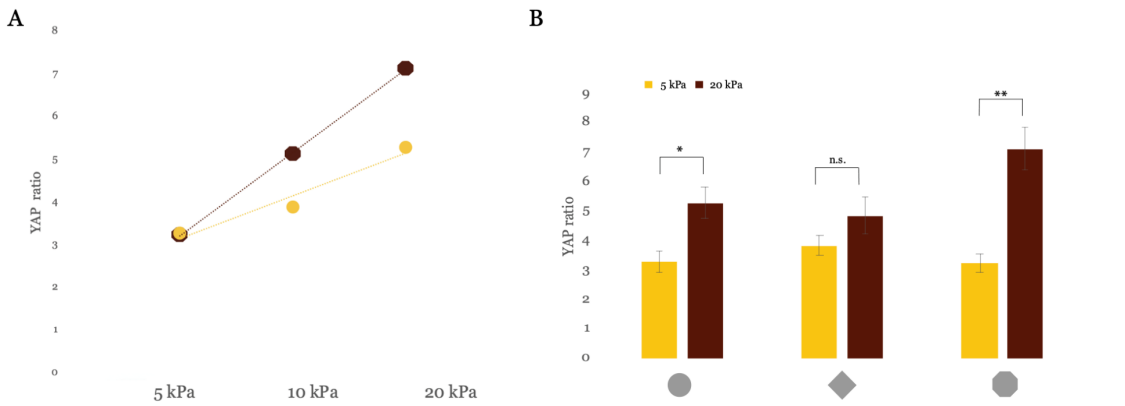

(A)

Note. YAP ratio shows linear increases across gels of different stiffness. YAP ratio of octagons increases with a greater slope than that of circles. (B) YAP ratio significantly increases across low (5 kPa) and high (20 kPa) stiffnesses for circles and octagons. Squares exhibit relatively similar levels of YAP on hydrogels of both stiffnesses.

Figure 17

Changes in Shape Among Octagons

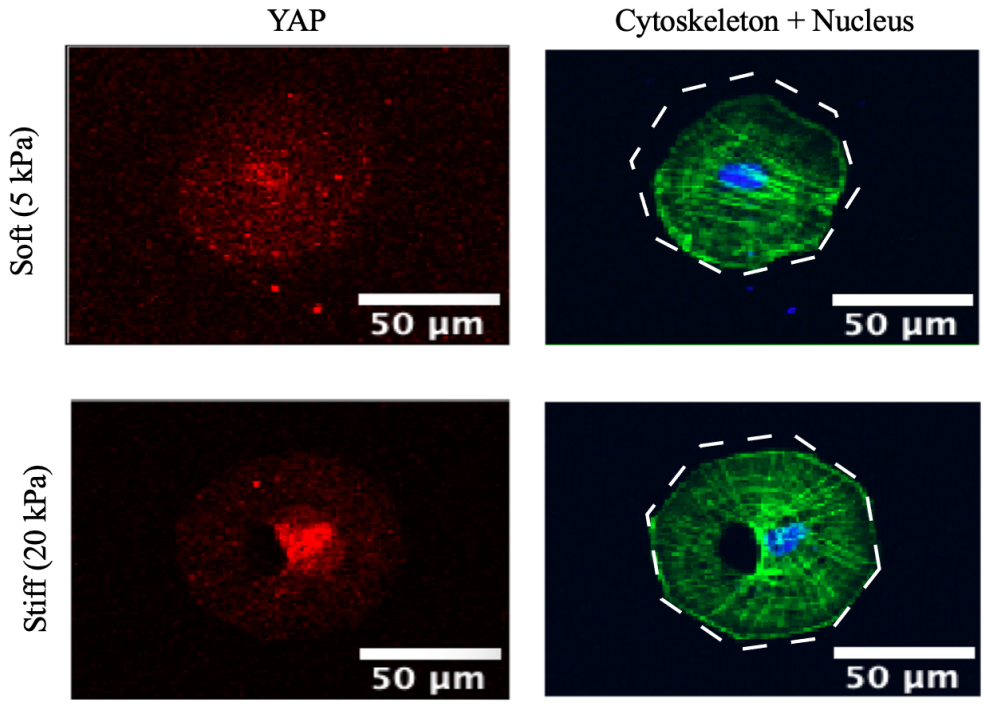

Note. Octagons on lower stiffnesses show more rounded edges with less clear vertices than those on stiff gels. Octagon pattern can be seen outlined in white around cells stained phalloidin (green) and Hoechst (blue) stains. The impact of this is reflected in corresponding YAP stains (red).

3.3.2.4 Stiffness and Shape Influence on Cell Adhesion. When imaging cells adhered to patterns, it was seen that cells on low stiffness gels were more often found in circular patterns and cells on higher stiffness gels were more often found on octagons (Figure 18). It is not known if cells sense their environment before adhesion and preferentially chose pattern shape, or if another factor is at play. Increased testing would need to be done to determine statistical relevance of these observations as well as if counts of cells in each shape each out with higher sample sizes.

Figure 18

Occurrence of Patterns in Relation to Stiffness

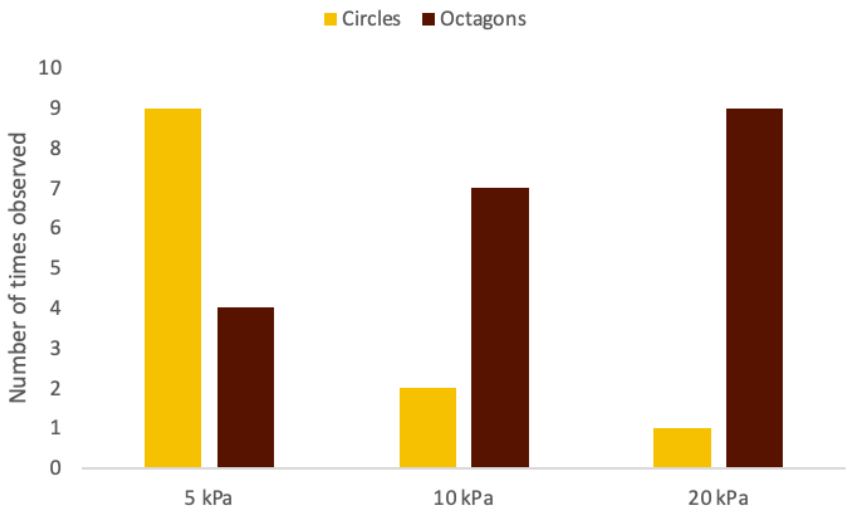

Note. Number of circles (yellow) and octagons (brown) seen across 3 stiffnesses.

Chapter 4

Summary and Future Directions

4.1 Summary

NorHA hydrogels of varying stiffness can be micropatterned with shapes without effecting stiffness [43]. Here it was shown that patterning on NorHA hydrogels is highly accurate when using a glass photomask and UV light. Average patterns on NorHA hydrogels were 95.6% the size of their photomask counterparts. Consistent pattern size allowed for the study of shape and stiffness with MSCs.

MSCs plated on patterned NorHA hydrogels exhibited varying levels of YAP concentrations. Circles plated on soft gels were seen to have the lowest YAP concentration while octagons on stiff gels had the highest YAP concentrations. Cells on squares were seen to have similar YAP ratios to those on octagons indicating the possibility if a maximum threshold of mechanosensing based off cytoskeletal contractility. Additionally, on hydrogels of a medium, 10 kPa, stiffness YAP concentrations increased from circle to octagon. This indicates that both stiffness and shape greatly effect mechanosensing.

When combined it was seen that shape and stiffness can have a greater impact on mechanosensing than either factor individually. Angular shapes on stiff gels resulted in higher cellular mechanosensing than just shape or stiffness alone. The opposite is also seen for circular shapes and soft gels as they decrease mechanosensing when used in combination. This effect of stiffness and shape on mechanosensing can be translated to effects on differentiation based on the known relationship between YAP mechanosensing and MSC differentiation [36]. Increased mechanosensing, seen here in angular stiff cells,

correlates to osteogenic differentiation while lower mechanosensing, seen here in round soft cells, correlates to adipogenic differentiation [30], [36].

4.2 Effect of Physical Cell-Cell Contact on Mechanosensing

4.2.1 How Cell-Cell Contact Effects Mechanosensing

In addition to the combinatorial effects of stiffness and shape not being well characterized, little is known about the effect of cell-cell contact on mechanosensing. Previous mechanosensing studies were done on single cell islands [36], [41], leaving out the impact of cell-cell contact on mechanosensing. At high densities, cell-cell contact is seen to inhibit osteogenesis due cells having less ECM-substrate contact and lower overall cell areas [30]. It has also been seen that changes in force can be relayed quickly through tissue cells [58], [59]. These high density and tissue studies have been done with multicell substrates [30], [59], again leaving little information on the effect of one cell on another when it comes to mechanosensing.

4.2.2 Use of this Biomaterial System to Study Cell-Cell Effect on Mechanosensing

The work done here has created a biomaterial system that can be used to test combinations of patterned shapes for better understanding of the effect of cell-cell contact on mechanosensing. Combinations of the same three main shapes have been made on a photomask to study this. These combinations include circle-circle, circle-square, circle-octagon, square-octagon, square-square and octagon-octagon (Figure 19A). The shapes are the same three as before that are known to exhibit a range of mechanosensing, but this time the impact of those different shapes can be seen on each other. These shapes will be used in the same way to pattern hydrogels and seed MSCs to determine the effect of cell-cell contact. Contact area between the shapes was kept consistent at 10 micrometers as

changes in cell contact area have been seen to influence amount of cell-cell signaling [60]. Cell seeding on these combinations of patterns will offer insight on the effect of cell- cell contact on mechanosensing, as well as how shape, cell-cell contact, and stiffness effect mechanosensing in conjunction.

4.2.3 Preliminary Findings

Preliminary work aims to find an adequate seeding density and culture time to obtain one cell in each shape (Figure 19B). Previous seeding densities for single shape patterns do not adequately fill conjoined shape patterns, but as seen in single cell tests it is easy to over seed cells and obtain clusters of cells in a pattern. Once this optimal seeding density is achieved, YAP ratio characterization can be done just as it was previously to determine the influence of cell-cell contact on mechanosensing as well the influence of cell-cell contact in combination with shape and stiffness variations.

Figure 19

Cell-Cell Contact Photomask Design

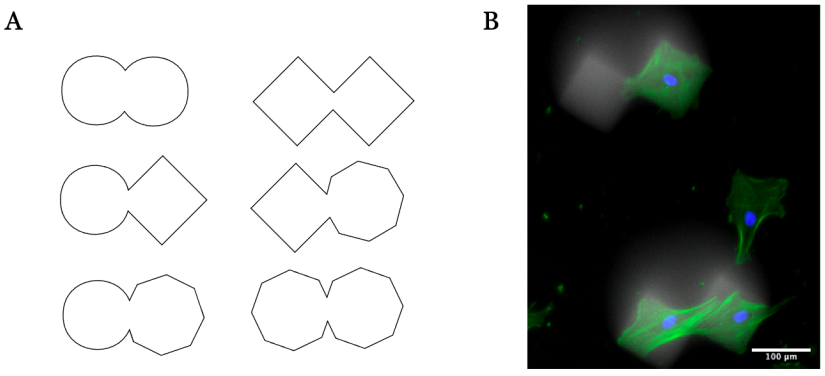

Note. (A) Outline of conjoined shapes for photomask (B) Cells seeded on conjoined shapes

4.3 Effect of Engineered Cell-Cell Contact on Mechanosensing

Once cell-cell contact on mechanosensing is better understood, it can be manipulated to further study its effect on mechanosensing. Cell-cell contact in MSCs is regulated by N-cadherin binding between cells. N-cadherin has an extracellular domain to bind cells together and an intracellular domain for signaling to and from adjoining cells [61]. A synthetically engineered N-cadherin mimetic peptide 'HAVDI' has been shown to bind N-cadherin and influence MSC differentiation by allowing cells to believe they are adhered to another cell [62]. Success with this peptide has been able hinder focal adhesions and decrease nuclear localization of YAP [63]. Inclusion of HAVDI peptide with single shape patterns previously used in this study would allow a better looks at the impact HAVDI has on YAP mechanosensing on cells of different shapes and stiffness as well as compared to cells in contact with one and other.

References

[1] W. Zakrzewski, M. Dobrzyński, M. Szymonowicz, and Z. Rybak, "Stem cells: past, present, and future," *Stem Cell Research & Therapy*, vol. 10, no. 1, p. 68, Feb. 2019, doi: 10.1186/s13287-019-1165-5.

[2] D. van der Kooy and and S. Weiss, "Why Stem Cells?," *Science*, vol. 287, no. 5457, pp. 1439–1441, Feb. 2000, doi: 10.1126/science.287.5457.1439.

[3] University of Nebraska Medical Center, "Types of Stem Cell | Stem Cells | University of Nebraska Medical Center," 2020. https://www.unmc.edu/stemcells/educational-resources/types.html (accessed May 01, 2021).

[4] A. E. Bishop, L. D. K. Buttery, and J. M. Polak, "Embryonic stem cells," *The Journal of Pathology*, vol. 197, no. 4, pp. 424–429, 2002, doi: https://doi.org/10.1002/path.1154.

[5] M. Kassem, "Stem cells: potential therapy for age-related diseases," *Ann N Y Acad Sci*, vol. 1067, pp. 436–442, May 2006, doi: 10.1196/annals.1354.062.

[6] H. J. Rippon and A. E. Bishop, "Embryonic stem cells," *Cell Proliferation*, vol. 37, no. 1, pp. 23–34, 2004, doi: https://doi.org/10.1111/j.1365-2184.2004.00298.x.

[7] J. M. Moraleda *et al.*, "Adult stem cell therapy: Dream or reality?," *Transplant Immunology*, vol. 17, no. 1, pp. 74–77, Dec. 2006, doi: 10.1016/j.trim.2006.09.030.

[8] D. Clarke and J. Frisén, "Differentiation potential of adult stem cells," *Current Opinion in Genetics & Development*, vol. 11, no. 5, pp. 575–580, Oct. 2001, doi: 10.1016/S0959-437X(00)00235-5.

[9] S. Temple, "The development of neural stem cells," *Nature*, vol. 414, no. 6859, Art. no. 6859, Nov. 2001, doi: 10.1038/35102174.

[10] S. Pluchino, L. Zanotti, M. Deleidi, and G. Martino, "Neural stem cells and their use as therapeutic tool in neurological disorders," *Brain Research Reviews*, vol. 48, no. 2, pp. 211–219, Apr. 2005, doi: 10.1016/j.brainresrev.2004.12.011.

[11] M. F. Pittenger *et al.*, "Multilineage Potential of Adult Human Mesenchymal Stem Cells," *Science*, vol. 284, no. 5411, pp. 143–147, Apr. 1999, doi: 10.1126/science.284.5411.143.

[12] A. I. Caplan, "Mesenchymal stem cells," *Journal of Orthopaedic Research*, vol. 9, no. 5, pp. 641–650, 1991, doi: https://doi.org/10.1002/jor.1100090504.

[13] E. Yamachika *et al.*, "Basic fibroblast growth factor supports expansion of mouse compact bone-derived mesenchymal stem cells (MSCs) and regeneration of bone from MSC in vivo," *J Mol Hist*, vol. 43, no. 2, pp. 223–233, Apr. 2012, doi: 10.1007/s10735-011-9385-8.

[14] G. Filardo, F. Perdisa, A. Roffi, M. Marcacci, and E. Kon, "Stem cells in articular cartilage regeneration," *J Orthop Surg Res*, vol. 11, no. 1, p. 42, Apr. 2016, doi: 10.1186/s13018-016-0378-x.

[15] S. J. Szilvassy, "The biology of hematopoietic stem cells," *Archives of Medical Research*, vol. 34, no. 6, pp. 446–460, Nov. 2003, doi: 10.1016/j.arcmed.2003.06.004.

[16] K. Takahashi and S. Yamanaka, "Induction of Pluripotent Stem Cells from Mouse Embryonic and Adult Fibroblast Cultures by Defined Factors," *Cell*, vol. 126, no. 4, pp. 663–676, Aug. 2006, doi: 10.1016/j.cell.2006.07.024.

[17] D. A. Robinton and G. Q. Daley, "The promise of induced pluripotent stem cells in research and therapy," *Nature*, vol. 481, no. 7381, Art. no. 7381, Jan. 2012, doi: 10.1038/nature10761.

[18] A. Morizane *et al.*, "Direct Comparison of Autologous and Allogeneic Transplantation of iPSC-Derived Neural Cells in the Brain of a Nonhuman Primate," *Stem Cell Reports*, vol. 1, no. 4, pp. 283–292, Oct. 2013, doi: 10.1016/j.stemcr.2013.08.007.

[19] M. Rao, "iPSC-Based Cell Therapy: An Important Step Forward," *Stem Cell Reports*, vol. 1, no. 4, pp. 281–282, Oct. 2013, doi: 10.1016/j.stemcr.2013.10.002.

[20] J. A. Burdick and G. Vunjak-Novakovic, "Engineered Microenvironments for Controlled Stem Cell Differentiation," *Tissue Engineering Part A*, vol. 15, no. 2, pp. 205–19, Feb. 2009, doi: http://dx.doi.org.ezproxy.rowan.edu/10.1089/ten.tea.2008.0131.

[21] E. Dawson, G. Mapili, K. Erickson, S. Taqvi, and K. Roy, "Biomaterials for stem cell differentiation," *Advanced Drug Delivery Reviews*, vol. 60, no. 2, pp. 215–228, Jan. 2008, doi: 10.1016/j.addr.2007.08.037.

[22] National Institute of Biomedical Imaging and Bioengineering, "Biomaterials," *nibib.nih.gov*, Sep. 2017. https://www.nibib.nih.gov/science-education/science-topics/biomaterials (accessed Apr. 30, 2021).

[23] J. Kopeček, "Hydrogel biomaterials: A smart future?," *Biomaterials*, vol. 28, no. 34, pp. 5185–5192, Dec. 2007, doi: 10.1016/j.biomaterials.2007.07.044.

[24] M. W. Tibbitt and K. S. Anseth, “Hydrogels as Extracellular Matrix Mimics for 3D Cell Culture,” *Biotechnol Bioeng*, vol. 103, no. 4, pp. 655–663, Jul. 2009, doi: 10.1002/bit.22361.

[25] D. Seliktar, “Designing Cell-Compatible Hydrogels for Biomedical Applications,” *Science*, vol. 336, no. 6085, pp. 1124–1128, Jun. 2012, doi: 10.1126/science.1214804.

[26] L. S. Ferreira, S. Gerecht, J. Fuller, H. F. Shieh, G. Vunjak-Novakovic, and R. Langer, “Bioactive hydrogel scaffolds for controllable vascular differentiation of human embryonic stem cells,” *Biomaterials*, vol. 28, no. 17, pp. 2706–2717, Jun. 2007, doi: 10.1016/j.biomaterials.2007.01.021.

[27] D. S. W. Benoit, M. P. Schwartz, A. R. Durney, and K. S. Anseth, “Small molecule functional groups for the controlled differentiation of human mesenchymal stem cells encapsulated in poly(ethylene glycol) hydrogels,” *Nat Mater*, vol. 7, no. 10, pp. 816–823, Oct. 2008, doi: 10.1038/nmat2269.

[28] A. J. Engler, S. Sen, H. L. Sweeney, and D. E. Discher, “Matrix Elasticity Directs Stem Cell Lineage Specification,” *Cell*, vol. 126, no. 4, pp. 677–689, Aug. 2006, doi: 10.1016/j.cell.2006.06.044.

[29] W. Farhat, A. Hasan, L. Lucia, F. Becquart, A. Ayoub, and F. Kobeissy, “Hydrogels for Advanced Stem Cell Therapies: A Biomimetic Materials Approach for Enhancing Natural Tissue Function,” *IEEE Reviews in Biomedical Engineering*, vol. 12, pp. 333–351, 2019, doi: 10.1109/RBME.2018.2824335.

[30] R. McBeath, D. M. Pirone, C. M. Nelson, K. Bhadriraju, and C. S. Chen, “Cell shape, cytoskeletal tension, and RhoA regulate stem cell lineage commitment,” *Dev Cell*, vol. 6, no. 4, pp. 483–495, Apr. 2004, doi: 10.1016/s1534-5807(04)00075-9.

[31] D. E. Jaalouk and J. Lammerding, “Mechanotransduction gone awry,” *Nature Reviews Molecular Cell Biology*, vol. 10, no. 1, Art. no. 1, Jan. 2009, doi: 10.1038/nrm2597.

[32] M. Brosig, J. Ferralli, L. Gelman, M. Chiquet, and R. Chiquet-Ehrismann, “Interfering with the connection between the nucleus and the cytoskeleton affects nuclear rotation, mechanotransduction and myogenesis,” *The International Journal of Biochemistry & Cell Biology*, vol. 42, no. 10, pp. 1717–1728, Oct. 2010, doi: 10.1016/j.biocel.2010.07.001.

[33] B. Geiger, J. P. Spatz, and A. D. Bershadsky, “Environmental sensing through focal adhesions,” *Nature Reviews Molecular Cell Biology*, vol. 10, no. 1, Art. no. 1, Jan. 2009, doi: 10.1038/nrm2593.

[34] G. R. Fedorchak, A. Kaminski, and J. Lammerding, “Cellular mechanosensing: Getting to the nucleus of it all,” *Progress in Biophysics and Molecular Biology*, vol. 115, no. 2, pp. 76–92, Aug. 2014, doi: 10.1016/j.pbiomolbio.2014.06.009.

[35] L. R. Smith, S. Cho, and D. E. Discher, “Stem Cell Differentiation is Regulated by Extracellular Matrix Mechanics,” *Physiology*, vol. 33, no. 1, pp. 16–25, Dec. 2017, doi: 10.1152/physiol.00026.2017.

[36] A. S. Mao, J.-W. Shin, and D. J. Mooney, “Effects of substrate stiffness and cell-cell contact on mesenchymal stem cell differentiation,” *Biomaterials*, vol. 98, pp. 184–191, Aug. 2016, doi: 10.1016/j.biomaterials.2016.05.004.

[37] C. Lorthongpanich *et al.*, “YAP as a key regulator of adipo-osteogenic differentiation in human MSCs,” *Stem Cell Research & Therapy*, vol. 10, no. 1, p. 402, Dec. 2019, doi: 10.1186/s13287-019-1494-4.

[38] S. Dupont, “Role of YAP/TAZ in cell-matrix adhesion-mediated signalling and mechanotransduction,” *Experimental Cell Research*, vol. 343, no. 1, pp. 42–53, Apr. 2016, doi: 10.1016/j.yexcr.2015.10.034.

[39] O. Chaudhuri *et al.*, “Hydrogels with tunable stress relaxation regulate stem cell fate and activity,” *Nat Mater*, vol. 15, no. 3, pp. 326–334, Mar. 2016, doi: 10.1038/nmat4489.

[40] S. Huang, C. S. Chen, and D. E. Ingber, “Control of Cyclin D1, p27Kip1, and Cell Cycle Progression in Human Capillary Endothelial Cells by Cell Shape and Cytoskeletal Tension,” *MBoC*, vol. 9, no. 11, pp. 3179–3193, Nov. 1998, doi: 10.1091/mbc.9.11.3179.

[41] K. A. Kilian, B. Bugarija, B. T. Lahn, and M. Mrksich, “Geometric cues for directing the differentiation of mesenchymal stem cells,” *Proc Natl Acad Sci USA*, vol. 107, no. 11, p. 4872, Mar. 2010, doi: 10.1073/pnas.0903269107.

[42] S. Dupont *et al.*, “Role of YAP/TAZ in mechanotransduction,” *Nature*, vol. 474, no. 7350, Art. no. 7350, Jun. 2011, doi: 10.1038/nature10137.

[43] W. M. Gramlich, I. L. Kim, and J. A. Burdick, “Synthesis and orthogonal photopatterning of hyaluronic acid hydrogels with thiol-norbornene chemistry,” *Biomaterials*, vol. 34, no. 38, pp. 9803–9811, Dec. 2013, doi: 10.1016/j.biomaterials.2013.08.089.

[44] S. R. Caliari, S. L. Vega, M. Kwon, E. M. Soulas, and J. A. Burdick, “Dimensionality and spreading influence MSC YAP/TAZ signaling in hydrogel environments,” *Biomaterials*, vol. 103, pp. 314–323, Oct. 2016, doi: 10.1016/j.biomaterials.2016.06.061.

[45] Taekehisa Matsuda, Kazuhiko Inoue, and Takashi Sugawara, “Development of Micropatterning Technology for Cultured Cells,” *Biomaterials*, vol. 36, no. American Society iof Artifical Internal Organs, pp. M559–M562, Sep. 1990.

[46] M. Théry, “Micropatterning as a tool to decipher cell morphogenesis and functions,” *Journal of Cell Science*, vol. 123, no. 24, pp. 4201–4213, Dec. 2010, doi: 10.1242/jcs.075150.

[47] C. J. Poon *et al.*, “Preparation of an adipogenic hydrogel from subcutaneous adipose tissue,” *Acta Biomaterialia*, vol. 9, no. 3, pp. 5609–5620, Mar. 2013, doi: 10.1016/j.actbio.2012.11.003.

[48] N. Huebsch *et al.*, “Harnessing traction-mediated manipulation of the cell/matrix interface to control stem-cell fate,” *Nature Materials*, vol. 9, no. 6, Art. no. 6, Jun. 2010, doi: 10.1038/nmat2732.

[49] C. H. Turner, J. Rho, Y. Takano, T. Y. Tsui, and G. M. Pharr, “The elastic properties of trabecular and cortical bone tissues are similar: results from two microscopic measurement techniques,” *Journal of Biomechanics*, vol. 32, no. 4, pp. 437–441, Apr. 1999, doi: 10.1016/S0021-9290(98)00177-8.

[50] E. Eggenhofer, F. Luk, M. H. Dahlke, and M. J. Hoogduijn, “The Life and Fate of Mesenchymal Stem Cells,” *Front. Immunol.*, vol. 5, 2014, doi: 10.3389/fimmu.2014.00148.

[51] D. J. Prockop, “Marrow Stromal Cells as Stem Cells for Nonhematopoietic Tissues,” *Science*, vol. 276, no. 5309, pp. 71–74, Apr. 1997, doi: 10.1126/science.276.5309.71.

[52] E. D. Prè, G. Conti, and A. Sbarbati, “Hyaluronic Acid (HA) Scaffolds and Multipotent Stromal Cells (MSCs) in Regenerative Medicine,” *Stem Cell Rev and Rep*, vol. 12, no. 6, pp. 664–681, Dec. 2016, doi: 10.1007/s12015-016-9684-2.

[53] M. E. Bernardo, D. Pagliara, and F. Locatelli, “Mesenchymal stromal cell therapy: a revolution in Regenerative Medicine?,” *Bone Marrow Transplantation*, vol. 47, no. 2, Art. no. 2, Feb. 2012, doi: 10.1038/bmt.2011.81.

[54] D. Cook and P. Genever, “Regulation of Mesenchymal Stem Cell Differentiation,” in *Transcriptional and Translational Regulation of Stem Cells*, G. Hime and H. Abud, Eds. Dordrecht: Springer Netherlands, 2013, pp. 213–229. doi: 10.1007/978-94-007-6621-1_12.

[55] A. I. Caplan and S. P. Bruder, “Mesenchymal stem cells: building blocks for molecular medicine in the 21st century,” *Trends Mol Med*, vol. 7, no. 6, pp. 259–264, Jun. 2001, doi: 10.1016/s1471-4914(01)02016-0.

[56] S. Piccolo, S. Dupont, and M. Cordenonsi, "The Biology of YAP/TAZ: Hippo Signaling and Beyond," *Physiological Reviews*, vol. 94, no. 4, pp. 1287–1312, Oct. 2014, doi: 10.1152/physrev.00005.2014.

[57] R. Johnson and G. Halder, "The two faces of Hippo: targeting the Hippo pathway for regenerative medicine and cancer treatment," *Nat Rev Drug Discov*, vol. 13, no. 1, pp. 63–79, Jan. 2014, doi: 10.1038/nrd4161.

[58] J. Howard, S. W. Grill, and J. S. Bois, "Turing's next steps: the mechanochemical basis of morphogenesis," *Nature Reviews Molecular Cell Biology*, vol. 12, no. 6, Art. no. 6, Jun. 2011, doi: 10.1038/nrm3120.

[59] A. S. Yap, K. Duszyc, and V. Viasnoff, "Mechanosensing and Mechanotransduction at Cell–Cell Junctions," *Cold Spring Harb Perspect Biol*, vol. 10, no. 8, p. a028761, Aug. 2018, doi: 10.1101/cshperspect.a028761.

[60] O. Shaya *et al.*, "Cell-Cell Contact Area Affects Notch Signaling and Notch-Dependent Patterning," *Developmental Cell*, vol. 40, no. 5, pp. 505-511.e6, Mar. 2017, doi: 10.1016/j.devcel.2017.02.009.

[61] B. M. Gumbiner, "Regulation of cadherin-mediated adhesion in morphogenesis," *Nature Reviews Molecular Cell Biology*, vol. 6, no. 8, Art. no. 8, Aug. 2005, doi: 10.1038/nrm1699.

[62] L. Bian, M. Guvendiren, R. L. Mauck, and J. A. Burdick, "Hydrogels that mimic developmentally relevant matrix and N-cadherin interactions enhance MSC chondrogenesis," *Proc Natl Acad Sci U S A*, vol. 110, no. 25, pp. 10117–10122, Jun. 2013, doi: 10.1073/pnas.1214100110.

[63] B. D. Cosgrove *et al.*, "N-cadherin adhesive interactions modulate matrix mechanosensing and fate commitment of mesenchymal stem cells," *Nature Materials*, vol. 15, no. 12, Art. no. 12, Dec. 2016, doi: 10.1038/nmat4725.